

## THE WFC3 GALACTIC BULGE TREASURY PROGRAM: A FIRST LOOK AT RESOLVED STELLAR POPULATION TOOLS

THOMAS M. BROWN<sup>1</sup>, KALASH SAHU<sup>1</sup>, MANUELA ZOCCALI<sup>2</sup>, ALVIO RENZINI<sup>3</sup>, HENRY C. FERGUSON<sup>1</sup>, JAY ANDERSON<sup>1</sup> ED SMITH<sup>1</sup>, HOWARD E. BOND<sup>1</sup>, DANTE MINNITI<sup>2,4</sup>, JEFF A. VALENTI<sup>1</sup>, STEFANO CASERTANO<sup>1</sup>, MARIO LIVIO<sup>1</sup>, NINO PANAGIA<sup>1</sup>, DON A. VANDENBERG<sup>5</sup>, ELENA VALENTI<sup>6</sup>,

*To appear in The Astronomical Journal*

### ABSTRACT

When the Wide Field Camera 3 (WFC3) is installed on the *Hubble Space Telescope (HST)*, the community will have access to powerful new capabilities for investigating resolved stellar populations. The WFC3 Galactic Bulge Treasury program will obtain deep imaging in five photometric bands on four low-extinction fields. These data will have no proprietary period, and will enable a variety of science investigations not possible with previous data sets. To aid in planning for the use of these data and for future observing proposals, we provide an introduction to the Treasury program, its photometric system, and the associated calibration effort.

The observing strategy is based upon a new photometric system employing five WFC3 bands spanning the UV, optical, and near-infrared: F390W, F555W, F814W, F110W, and F160W (analogous but not identical to the ground-based filters Washington *C, V, I, J*, and *H*). With these bands, one can construct reddening-free indices of temperature and metallicity. Using this photometric system, the program will target six fields in well-studied star clusters, spanning a wide range of metallicity, and four fields in low-extinction windows of the Galactic bulge. The cluster data serve to calibrate the reddening-free indices, provide empirical population templates, and correct the transformation of theoretical isochrone libraries into the WFC3 photometric system. The bulge data will shed light on the bulge formation history, and will also serve as empirical population templates for other studies. One of the fields includes 12 candidate hosts of extrasolar planets.

Color-magnitude diagrams (CMDs) are the most popular tool for analyzing resolved stellar populations. However, due to degeneracies among temperature, metallicity, and reddening in traditional CMDs, it can be difficult to draw robust conclusions from the data. The five-band system used for the bulge Treasury observations will provide reddening-free indices that are roughly orthogonal in temperature and metallicity, and we argue that model fitting in an index-index diagram will make better use of the information than fitting separate CMDs. We provide some results from simulations to show the expected quality of the data and their potential for differentiating between different star-formation histories.

**Subject headings:** Galaxy: bulge – Galaxy: formation – Galaxy: stellar content – stars: low-mass – globular clusters: individual (M92, NGC6752, 47 Tuc, NGC5927, NGC6528, NGC6791) – techniques: photometric

### 1. INTRODUCTION

The Wide Field Camera 3 (WFC3) is scheduled to be installed on the *Hubble Space Telescope (HST)* during the next servicing mission. Although the camera is intended as a general-purpose instrument, it offers particularly powerful new capabilities for studying resolved stellar populations. The camera will provide wide-field high-resolution imaging with continuous spectral coverage from the ultraviolet into the near-infrared through a choice of 77 filters and 3 grisms. Because it will be the first *HST* instrument to provide wide-field imaging in the near-infrared, an obvious target for WFC3 is the Galactic bulge, given its high reddening and crowding.

<sup>1</sup> Space Telescope Science Institute, 3700 San Martin Drive, Baltimore, MD 21218; tbrown@stsci.edu, ksahu@stsci.edu, ferguson@stsci.edu, jayand@stsci.edu, edsmith@stsci.edu, bond@stsci.edu, valenti@stsci.edu, stefano@stsci.edu, mlivio@stsci.edu, panagia@stsci.edu

<sup>2</sup> P. Universidad Católica de Chile, Departamento de Astronomía y Astrofísica, Casilla 306, Santiago 22, Chile; mzoccali@astro.puc.cl, dante@astro.puc.cl

<sup>3</sup> Osservatorio Astronomico, Vicoletto Dell'Osservatorio 5, I-35122 Padova, Italy; alvio.renzini@oapd.inaf.it

<sup>4</sup> Vatican Observatory, V-00120 Vatican City State, Italy

<sup>5</sup> Department of Physics and Astronomy, University of Victoria, P.O. Box 3055, Victoria, BC, V8W 3P6, Canada; davb@uvvm.uvic.ca

<sup>6</sup> European Southern Observatory, Alonso de Cordova 3107, Vitacura, Santiago, Chile; evalenti@eso.org

We describe here an observing technique that employs five WFC3 bands to create reddening-free indices of temperature and metallicity that can be used to explore a highly reddened and complex stellar population, such as the bulge.

The tools and techniques needed for a bulge investigation should be useful to a wider range of resolved stellar population studies, and a large database of bulge stars with reliable parameters (temperature, metallicity, proper motion, etc.) can enable additional observing programs directed specifically at the bulge, from both ground and space. These factors drove the creation of a bulge Treasury program (GO-11664), where all of the tools and products would be non-proprietary. The primary purpose of this paper is to demonstrate the general utility of the program's population tools (§2), which include photometry of six star clusters that can be used as empirical population templates (§2.3). In addition, this paper summarizes the scientific goals and data products specific to the Galactic bulge (§3). That description of the bulge investigation also motivates the development of the tools, provides concrete examples of how they can be used in stellar population studies, and enables future bulge studies. An early look at the program and its products allows them to be considered in the planning of observing proposals for upcoming *HST* cycles.

## 2. A NEW PHOTOMETRIC SYSTEM FOR HST

### 2.1. Reddening-Free Indices

Using techniques similar to those developed decades ago (e.g., Johnson & Morgan 1953; Strömgren 1966), we have constructed reddening-free indices of  $T_{\text{eff}}$  and metallicity combining five WFC3 filters (Figure 1): F390W, F555W, F814W, F110W, and F160W. For simplicity, these bands will hereafter be designated by names reflecting their ground-based analogs (Washington  $C$ ,  $V$ ,  $I$ ,  $J$ , and  $H$ ), and all of the magnitudes will be relative to Vega. Although the focus here is on the specific bandpasses of the WFC3, these photometric methods could in principle employ ground-based photometry in similar bandpasses; however, we note that the calibration of the indices for WFC3 will not be exactly the same as that for other observatories.

The usual practice for deriving a star formation history from such photometry would involve the construction of color-magnitude diagrams (CMDs). In a complex stellar population hosting a mix of ages and metallicities, this practice can provide the distributions in age and metallicity in a statistical sense. However, these five bandpasses go beyond such population fits to enable accurate measurements of  $T_{\text{eff}}$  and metallicity for *individual* stars. Although originating much earlier (Strömgren 1966 and references therein), the methodology is explained well by Mihalas & Binney (1981), and briefly summarized here. A reddening-free index combining three filters takes the form of

$$[c] = (m_1 - m_2) - (m_2 - m_3) \times \frac{E(m_1 - m_2)}{E(m_2 - m_3)} \quad (1)$$

where  $E(m_1 - m_2)$  is the excess in  $(m_1 - m_2)$  color due to extinction. Insensitivity to extinction requires that the ratio  $E(m_1 - m_2)/E(m_2 - m_3)$  be approximately constant with changes in stellar parameters. The choice of bands depends on the stellar parameter one is trying to constrain; in broad terms, bands spanning the optical to near-IR can constrain temperature from the peak and redward slope of the spectrum, while bands in the UV and optical can constrain the metallicity by exploiting UV absorption features. Guided by these facts, one can construct the following reddening-free indices of temperature and metallicity:

$$[t] = (V - J) - 5.75 \times (J - H) \quad (2)$$

and

$$[m] = (C - V) - 0.90 \times (V - I). \quad (3)$$

The coefficients come from an analysis of stellar isochrones (VandenBerg et al. 2006) folded through a library of synthetic spectra (Castelli & Kurucz 2003) and the response functions for each WFC3 filter (Figure 1), under different levels of assumed reddening (Fitzpatrick 1999). In Figure 2, we show the variation of these coefficients with surface gravity and effective temperature.

In practice, the coefficients, the relationship between  $[m]$  and  $[\text{Fe}/\text{H}]$ , and the relationship between  $[t]$  and  $T_{\text{eff}}$  should be calibrated using observations of well-studied star clusters, because the uncertainties are similar to those commonly found in the derivation of isochrone transformations. For example, when Brown et al. (2005) derived the transformation of theoretical isochrones into the bandpasses of the Advanced Camera for Surveys (ACS), they folded the Castelli & Kurucz (2003) spectra through the ACS response functions and found that an empirical color correction was required to align

the transformed isochrones with the observed CMDs of star clusters. The color of the red giant branch (RGB) at a given luminosity is a reddening-dependent indicator of metallicity, but the empirical correction to the transformation is required to use the RGB color in this manner. It was unclear how much of this correction was driven by uncertainties in the isochrones themselves, the synthetic spectra, or the response functions, but there will likely be similar issues with the transformation into WFC3 bandpasses.

Figures 3 and 4 demonstrate how these indices can be used to estimate effective temperature and metallicity even in the presence of significant reddening spreads and/or uncertainties. These figures split the population into dwarfs and giants for two reasons. The first reason is that dwarfs and giants overlap in a plane defined by temperature and metallicity, in contrast to a plane defined by temperature and luminosity (i.e., a CMD). Second, the reddening-free indices  $[m]$  and  $[t]$  are not completely insensitive to surface gravity; in particular, the relation between  $[m]$  and  $[\text{Fe}/\text{H}]$  is significantly distinct for dwarfs and giants. In general, an uncertainty of  $\sim 0.1$  mag in each index provides uncertainties of  $\lesssim 300$  K in effective temperature and 0.2 dex in  $[\text{Fe}/\text{H}]$ . The high gravity boundary in Figure 3 and the low gravity boundary in Figure 4 excludes stars below  $T_{\text{eff}} \lesssim 4000$  K, where the indices vary strongly with stellar parameters and the synthetic spectra are most prone to systematic errors; the indices for such cool stars will likely require significant calibration corrections using observations of stellar clusters. Because the coefficients in these indices are slowly varying functions of surface gravity (Figure 2), the estimates of effective temperature and metallicity are not particularly sensitive to distance uncertainties. One would use magnitude as a proxy for surface gravity when translating  $[m]$  to  $[\text{Fe}/\text{H}]$  and  $[t]$  to effective temperature (i.e., one can use position in a CMD to designate a star as a dwarf or giant and use the indices appropriately). In the bulge Treasury program, these indices will yield reliable estimates of metallicity and temperature for several tens of thousands of stars in a given WFC3 field, and do so in four fields; this will increase the number of bulge stars with such measurements by over two orders of magnitude. Although these indices are not direct age indicators, the temperature distribution in a resolved stellar population is a strong function of age. In the simulations below, we demonstrate how these diagrams can thus constrain the age distribution.

To find a photometric system that would be most useful for a broad range of stellar populations work, we folded the Victoria isochrone library (VandenBerg et al. 2006) through the entire WFC3 filter set, using the IRAF synphot package and the Castelli & Kurucz (2003) library of synthetic spectra. The search used five criteria: the filters must provide strong constraints on  $T_{\text{eff}}$  and  $[\text{Fe}/\text{H}]$ , they must provide such constraints despite significant distance and reddening uncertainties (enabling use in both clusters and field populations), the filters should be as broad as feasible (for observing efficiency), the number of filters should be minimized (for observing efficiency), and the bands should be as close as possible to standard photometric systems (to enable comparisons with both archival and future research). We explored many alternatives (e.g., narrower filters, alternative UV bands), but found that these were very inefficient for observing old (cool) stellar populations and/or highly reddened environments, and offered little improvement in the determination of  $[\text{Fe}/\text{H}]$  and  $T_{\text{eff}}$ . For example, one can construct a metallicity index that uses F336W (similar to  $U$ ) instead of F390W. To achieve

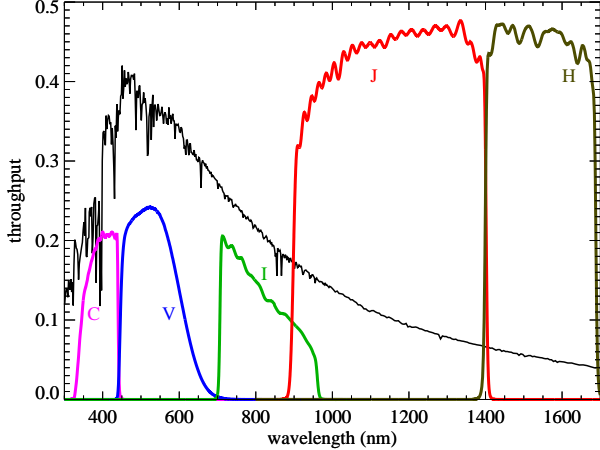


FIG. 1.— The system throughputs (colored curves) of the bandpasses employed in the bulge Treasury program: F390W (Washington C), F555W (V), F814W (I), F110W (wide J), and F160W (broad H). A solar analog spectrum (Castelli & Kurucz 2003; black curve) is shown for reference.

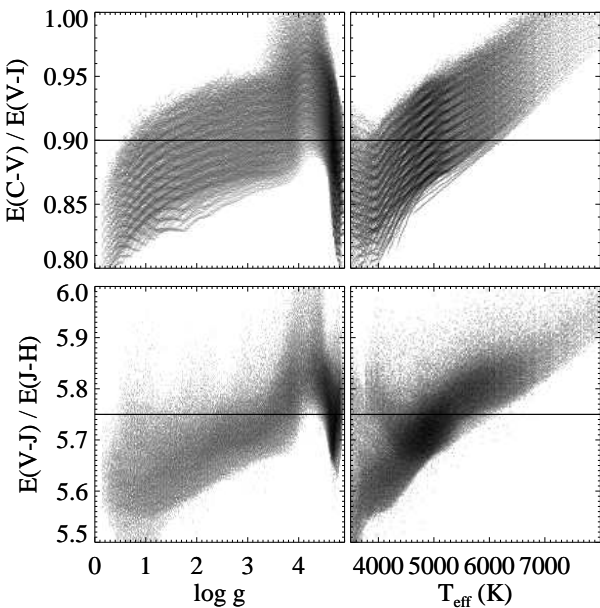


FIG. 2.— Color excess ratios as a function of stellar parameters, shown for isochrones (grey shading) spanning a range of age (4–14 Gyr), metallicity ( $-2.3 \leq [\text{Fe/H}] \leq 0.5$ ), and reddening ( $0 \leq A_V \leq 3.1$  mag). The values chosen for the coefficients in the reddening-free indices [m] and [t] are highlighted (black lines)

the same [Fe/H] accuracy with this alternative index as that achieved with the nominal [m] index above, the requirement on signal-to-noise in the F336W photometry is only half of that in the F390W photometry. However, for highly-reddened ( $A_V > 1.5$  mag) stars at cool temperatures ( $T_{\text{eff}} \lesssim 4500$  K), the observing time required to obtain such F336W photometry is over ten times longer than that needed to obtain the requisite F390W photometry.

The filters most commonly used for stellar populations work on the ACS were the F606W and F814W. While these filters are extremely efficient for observing faint stars, they are broad and not well-separated in wavelength. The WFC3 filters described here are not as efficient as the ACS ones, but they yield much stronger constraints on stellar parameters – breaking degeneracies between age, [Fe/H], and reddening (Figure 5). In their study of the stellar populations of An-

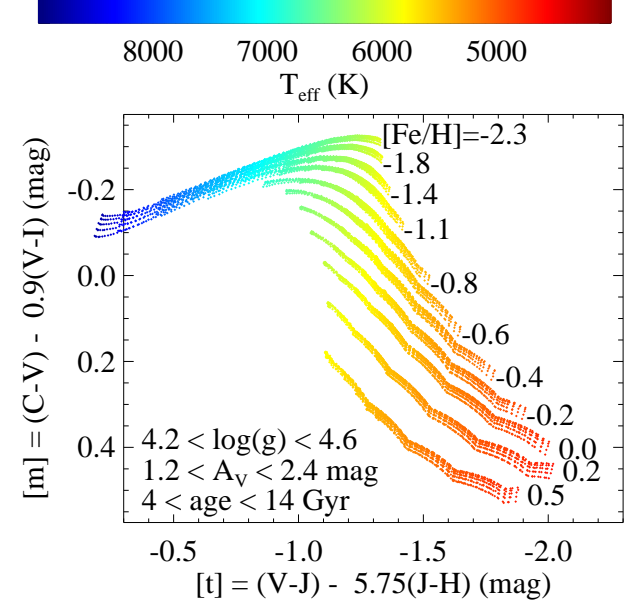


FIG. 3.— The distribution in the reddening-free indices [t] (temperature) and [m] (metallicity) for dwarf stars in a resolved stellar population spanning a wide range of age, extinction, and metallicity. Each band of points is labeled with the value of [Fe/H], while the colors indicate  $T_{\text{eff}}$ . The  $T_{\text{eff}}$  distribution at a given [Fe/H] is a strong function of age. The small spread in the band at each value of [Fe/H] comes from the fact that the indices are not perfectly insensitive to reddening. Nevertheless, this five-band system will provide sensitive tools for breaking the degeneracies between [Fe/H],  $T_{\text{eff}}$ , and extinction. Although analogous filters on the ground could be used to construct a similar diagram, it is worth noting that the calibration and coefficients would be distinct. Note that [t] becomes more positive with increasing temperature, opposite to colors such as  $B - V$ .

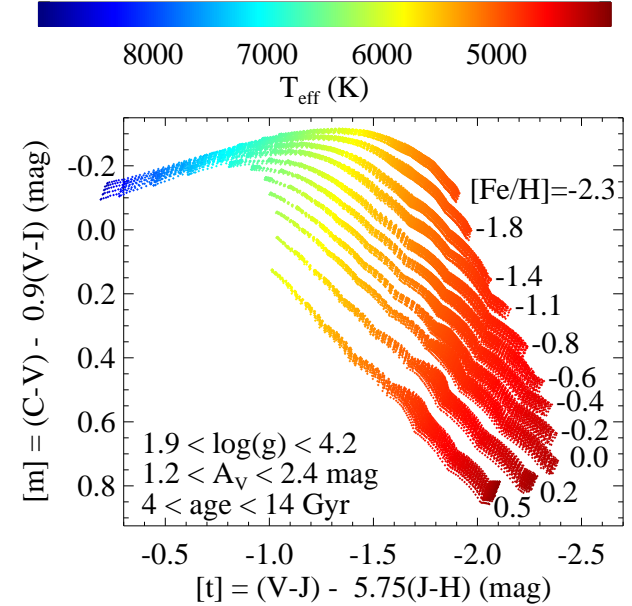


FIG. 4.— The same as in Figure 3, but for giant stars.

dromeda, Brown et al. (2006) explored the various systematic uncertainties pertinent to their ACS CMD analyses, and found that relatively small extinction uncertainties translated into relatively large age and [Fe/H] uncertainties.

A variety of CMDs can be constructed from these WFC3 filters, and they can all be fit simultaneously to yield the star-formation history in a stellar population (e.g., Figure 5). In the case of a simple stellar population, such fits use two fun-

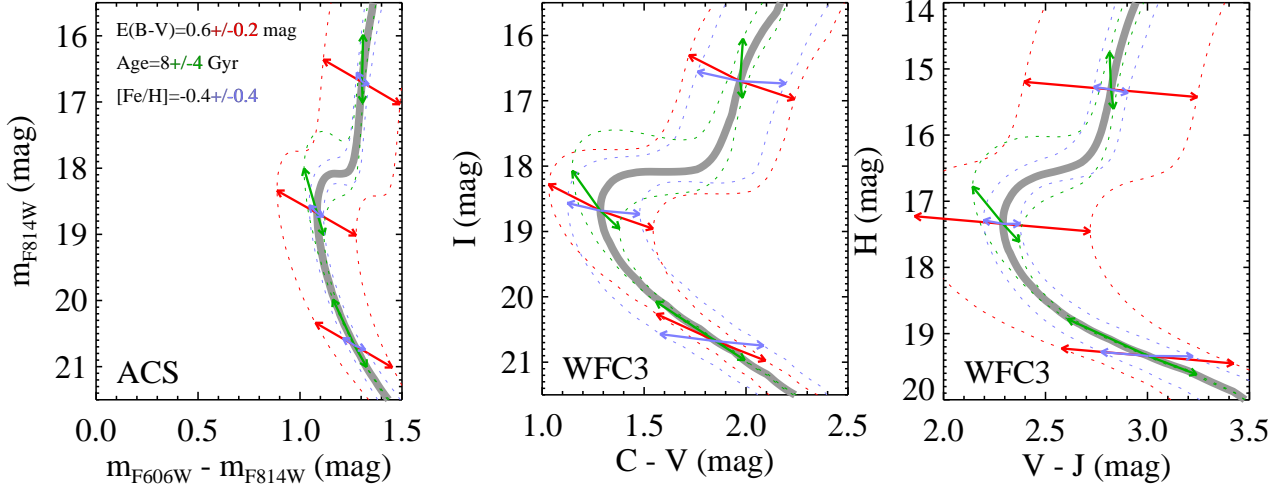


FIG. 5.— An isochrone for an 8 Gyr population with  $[Fe/H] = -0.4$  at 7.2 kpc with  $E(B-V) = 0.64$  mag (grey curve). Three positions are marked with arrows: the MSTO (bluest point on the main sequence), a point 2 mag brighter (on the RGB), and a point 2 mag fainter (on the main sequence). At each position, the colored arrows indicate how these positions would move in CMD space for changes in age (green),  $[Fe/H]$  (blue), and extinction (red). Dotted lines indicate how the entire isochrone would move. The RGB has little sensitivity to age, while the main sequence (below the MSTO) has no sensitivity to age, so the age shifts (green arrows) at these points are simply due to the fact that these points are defined relative to the luminosity of the MSTO, which is very sensitive to age. The left panel shows a CMD in the ACS F606W and F814W bands, while the middle and right panels show CMDs constructed from the WFC3 filters, with the same stretch on the axes. The WFC3 CMDs provide far better constraints on stellar parameters and break the degeneracies present in the ACS CMD. To recover the star-formation history in the bulge, one would fit the distributions in all five WFC3 filters simultaneously (not just the CMDs shown here).

damental clocks present in a CMD: the luminosity difference between the main sequence turnoff (MSTO) and horizontal branch (Sandage 1982; Iben & Renzini 1984), and the color difference between the MSTO and the red giant branch (VandenBerg et al. 1990). At fixed composition, the horizontal branch luminosity and red giant branch color are both relatively insensitive to age, while the MSTO becomes fainter and redder at increasing age. In the case of a complex stellar population such as a galaxy, CMD fitting (by Maximum Likelihood or  $\chi^2$  statistics) constrains the full two-dimensional distribution of age and  $[Fe/H]$  in a population, so that one can avoid assuming a single age-metallicity relationship (e.g., Dolphin 2002; Harris & Zaritsky 2001; Gallart et al. 1999; Holtzman et al. 1999; Brown et al. 2006; Cole et al. 2007). Such age-metallicity distributions can provide a definitive check on the chemical evolution models that have been used to explore the bulge formation history. It is worth stressing, however, that the advantage of the WFC3 five-band photometric system is that it can go beyond CMD fitting to constrain the  $T_{\text{eff}}$  and  $[Fe/H]$  of individual stars. The ability to measure these parameters independent of reddening can provide stronger constraints on the star formation history, as demonstrated below.

## 2.2. Simulated Populations

Figure 6 shows simulations of the planned bulge observations that demonstrate the sensitivity of this five-band photometry to the star-formation history. We simulated WFC3 images for each filter with realistic exposure times, backgrounds, noise, and crowding, and then blindly recovered the photometry using the DAOPHOT software of Stetson (1987). Despite the large spreads in assumed distance and extinction, an old population that formed over a period of several Gyr (*middle panels*) is easily distinguishable from one that formed in a nearly coeval burst (*bottom panels*). This particular simulation assumed the properties of the “SWEEPS” bulge field observed by Sahu et al. (2006) with the ACS, but the formation history will be distinguishable in each of the bulge fields being observed with WFC3. We have conservatively assumed the Dwek et al. (1995) bulge model to calculate the line-of-

sight distance spread, and the small variation in this spread from field to field. Measurements of the red clump luminosity within the SWEEPS field (Clarkson et al. 2008) demonstrate the spread is actually somewhat smaller ( $\sim 0.17$  mag instead of  $\sim 0.24$  mag), while ground-based surveys verify that the variation in spread is small ( $\lesssim 0.05$  mag) from field to field (Rattenbury et al. 2007).

Although it is clear in Figure 6 that a CMD such as  $I$  vs.  $V - H$  is sensitive to the star formation history, the use of five photometric filters provides much better constraints than available from traditional CMDs. With five bands, one really has a low-resolution spectrum of each star, and one can thus obtain better constraints on the physical parameters of interest (luminosity, temperature, and chemical composition), and then fit those to obtain the star formation history. When there are more than two photometric bands available, a common approach to fitting the star formation history is to simultaneously fit a series of CMDs constructed from combinations of those bands (e.g., Harris & Zaritsky 2004). However, such fitting of marginal distributions under-utilizes the information available, because it discards some of the photometric links for each star. The analogous situation for two-band photometry is the fitting of two distinct luminosity functions (which discards some information) instead of fitting a CMD (which preserves all information). For example, with the five WFC3 bands here, one could construct and simultaneously fit the following 4 CMDs:  $C$  vs.  $C - V$ ,  $V$  vs.  $V - I$ ,  $I$  vs  $I - J$ , and  $J$  vs.  $J - H$ . However, such a fit ignores the fact that a given star in  $C$  vs.  $C - V$  space has a specific position in  $J$  vs.  $J - H$  space. That star shows up in both CMDs, but the fact that it is the same star is not used. In contrast, if one simultaneously fits a series of  $[m]$  vs.  $[t]$  diagrams (where each diagram is taken from a cut in magnitude), then one is preserving the various photometric links for each star. If a red bandpass is used for the magnitude binning, this will minimize the uncertainties due to extinction, while the  $[m]$  and  $[t]$  indices are already insensitive to extinction. The magnitude bins can be chosen to emphasize particular stages of stellar evolution: bins spanning the main sequence (well below the MSTO) or the RGB

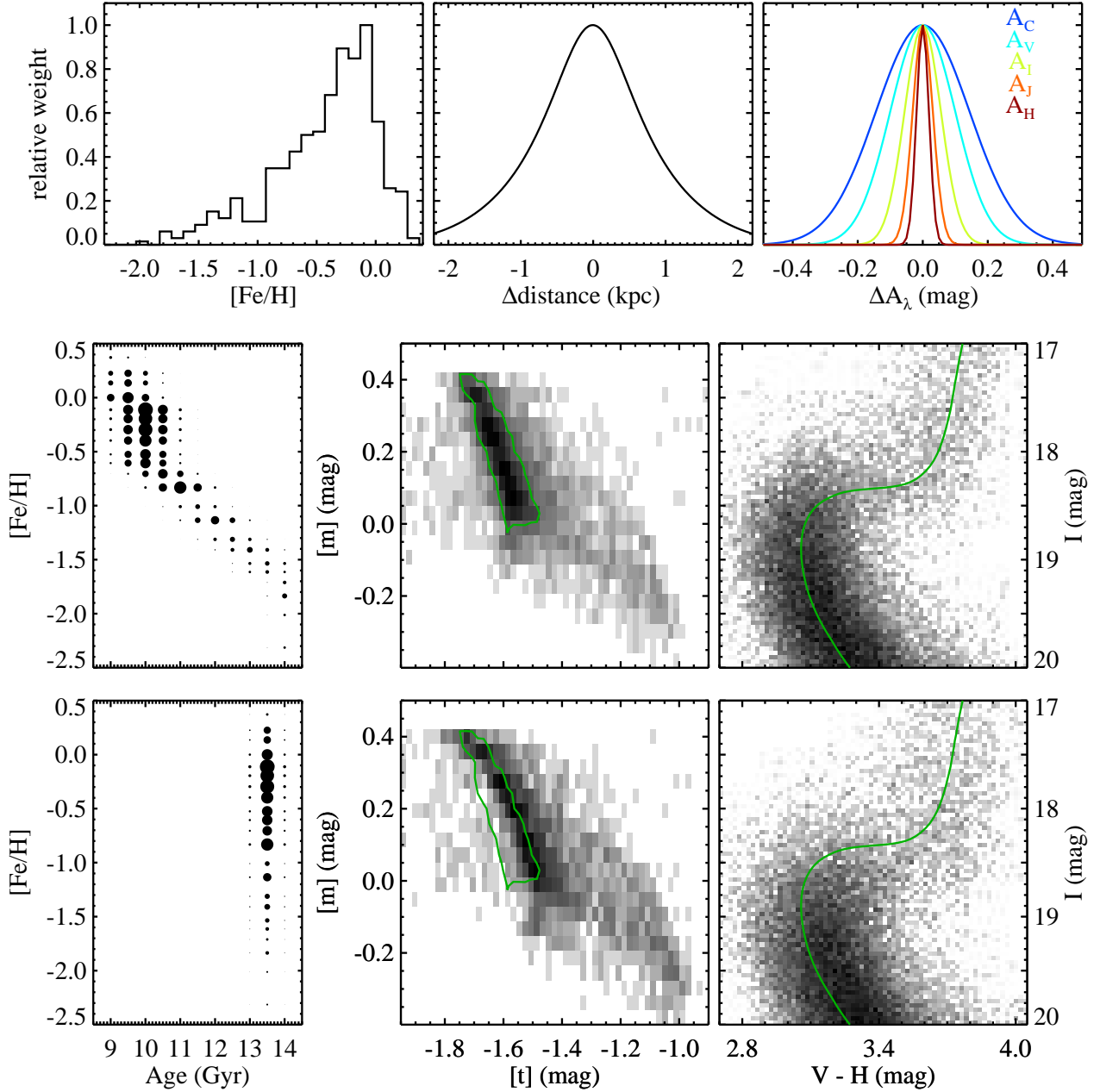


FIG. 6.— Simulations demonstrating how WFC3 bulge observations could distinguish between bulge formation scenarios. *Top row*: assumptions common to each simulation –  $[\text{Fe}/\text{H}]$  distribution (Zoccali et al. 2003), distance spread (Dwek et al. 1995), and extinction spread. *Middle row*: a simulated dataset arising from observations of a population with an extended star formation history, with the population used as input (left panel); area of filled circles proportional to the weight at the given age and  $[\text{Fe}/\text{H}]$ , and two diagrams constructed from the resulting photometry:  $[\text{m}]$  vs.  $[\text{t}]$  (middle panel; for stars at  $18 \leq I \leq 19$  mag), and  $I$  vs.  $V - H$  CMD (right panel). *Bottom row*: a simulated dataset arising from observations of an ancient population that formed in a nearly coeval burst, with the population used as input (left panel), the  $[\text{m}]$  vs.  $[\text{t}]$  diagram (middle panel;  $18 \leq I \leq 19$  mag) and  $I$  vs  $V - H$  CMD (right panel). In the  $[\text{m}]$  vs.  $[\text{t}]$  diagrams, the same contour (green curve) for the simulation in the middle row is shown for reference. In the  $I$  vs.  $V - H$  CMDs, the same isochrone (10 Gyr,  $[\text{Fe}/\text{H}] = -0.5$ ; green curve) is shown for reference. The  $[\text{m}]$  vs.  $[\text{t}]$  plots reflect the fact that the simulated populations have distinct temperature (and thus age) distributions but the same metallicity distributions.

(well above the subgiant branch) will give  $[\text{m}]$  vs.  $[\text{t}]$  diagrams that are primarily sensitive to  $[\text{Fe}/\text{H}]$ , while bins spanning the stars in the vicinity of the MSTO and subgiant branch (such as those in Figure 6) will be sensitive to both age and  $[\text{Fe}/\text{H}]$ .

Another way one can implement these reddening-free indices in a more traditional analysis is to apply  $[\text{Fe}/\text{H}]$  cuts (using  $[\text{m}]$ ) to the catalog before constructing CMDs. An example is shown in Figure 7. Here, we have taken the simulated populations of Figure 6 and divided each catalog into “high  $[\text{Fe}/\text{H}]$ ” and “low  $[\text{Fe}/\text{H}]$ ” bins, with a boundary at  $[\text{Fe}/\text{H}] \sim -0.8$  in the  $[\text{m}]$  vs.  $[\text{t}]$  plane. Because the primary

difference between the two simulated populations is a movement of metal-rich stars to intermediate ages, the shift in age (using the traditional indicators such as the luminosity of the MSTO and subgiant branch) is most apparent in the CMDs that use the  $[\text{m}]$  index to select metal-rich stars. Note that this technique is probably more useful for qualitative (i.e., by eye) evaluations of the star formation history instead of quantitative fitting. If one divided a catalog into metallicity bins using the  $[\text{m}]$  index, one could not simply fit each sub-catalog with a library of isochrones matching the same metallicity range implied by the index, because photometric scatter

TABLE 1  
GALACTIC CLUSTERS

Name	$(m - M)_V$ (mag)	$E(B - V)$ (mag)	[Fe/H] (Gyr)	age
NGC 6341 (M92)	14.60	0.023	-2.14	14.5
NGC 6752	13.17	0.055	-1.54	14.5
NGC 104 (47 Tuc)	13.27	0.024	-0.70	12.5
NGC 5927	15.85	0.42	-0.37	12.5
NGC 6528	16.31	0.55	+0.00	12.5
NGC 6791	13.50	0.14	+0.30	9.0

will allow some stars from outside each metallicity bin to leak into that metallicity bin. Thus, one would still need to fit the CMDs for each metallicity bin with an isochrone library spanning the full range of possible metallicities, subjected to the same culling in [m] vs. [t] space. For quantitative fitting, it is cleaner to fit a series of [m] vs. [t] diagrams in a series of appropriately chosen magnitude bins.

### 2.3. Empirical Population Templates

The bulge Treasury program includes observations of five Galactic globular clusters and one open cluster (Table 1; see Brown et al. 2005 and references therein for the evaluation of each cluster’s parameters). These clusters provide empirical population templates for direct comparison to the bulge data, enable an accurate transformation of theoretical isochrone libraries into the WFC3 photometric system, and allow the calibration of the new reddening-free indices of  $T_{\text{eff}}$  and metallicity. Existing synthetic spectral libraries are sufficiently accurate to demonstrate the potential of these indices, but application of this photometric system to real stellar populations will require direct calibration on well-studied clusters. These clusters were observed for a similar purpose in a series of Large ACS programs studying the populations of Andromeda (e.g., Brown et al. 2006); the cluster templates and isochrone transformations in the ACS bandpasses were provided to the community by Brown et al. (2005). The cluster templates, isochrone transformations, and population indices will be provided to the community as part of the bulge Treasury program.

## 3. SCIENCE GOALS OF THE TREASURY PROGRAM

### 3.1. The Formation History of the Bulge

We know little about the formation of galaxy bulges, due in part to the conflicting evidence about our own bulge, which is the one that can be studied in greatest detail (see Minniti & Zoccali 2007 for a review). From a populations perspective, the Galactic bulge looks like a “classical” bulge – i.e., similar to an old, nearly coeval elliptical galaxy. From a morphological perspective, the Galactic bulge looks like a “pseudo-bulge” – i.e., a peanut-shaped bulge apparently arising from bar-driven secular processes. As summarized by Kormendy & Kennicutt (2004), a range of physical processes may contribute to bulge formation, with rapid processes in discrete events (e.g., dissipative collapse, mergers of clouds and protogalaxies) dominating in the early universe, and slower secular processes (interactions between stars, gas clouds, bars, spiral structure, triaxial halos, etc.) dominating at later times. In broad terms, we see classical bulges if the earlier rapid processes are still dominant, while pseudo-bulges are thought to arise when the later slower processes are dominant. This discussion highlights a tension between observations and the framework of hierarchical galaxy formation. In general, semi-analytical models focus on the rapid processes relevant to

bulge formation, not on the slower secular process; however, even these models imply that spheroid formation occurs over billions of years – seemingly at odds with an old, nearly coeval spheroid (be it bulge, halo, or elliptical galaxy).

Color-magnitude diagrams of the Galactic bulge (e.g., Zoccali et al. 2003; Sahu et al. 2006) imply an old age ( $\gtrsim 10$  Gyr) with no detected trace of an intermediate-age population, but due to the age/metallicity/reddening degeneracies in the photometry obtained to date, it is unclear if the star-formation history in the bulge is somewhat extended (e.g., ages of 9–13 Gyr) or if it is restricted to a nearly coeval burst (e.g.,  $13 \pm 0.2$  Gyr). Given these limitations, researchers have also pursued a less direct approach to constraining the star-formation history of the bulge, by fitting chemical evolution models to the observed metallicity distribution in the population and the significant  $\alpha$ -element enhancement in individual stars (e.g., Ferreras et al. 2003; Ballero et al. 2007). These studies argue strongly that the bulge chemistry can be reproduced only if the period of star formation was shorter than 1 Gyr. Thus, both the CMD analyses (with large uncertainties) and chemical evolution models (with indirect constraints) are consistent with a classical bulge hosting an old, nearly coeval population. Such a brief burst of star formation argues against any significant contribution from the disk or even any protracted period of hierarchical merging. Semi-analytic models generally imply that bulges in galaxies like the Milky Way form over an extended period; e.g., if one looks at Milky Way analogs in the Millennium Simulation Project (De Lucia & Baizot 2007; Springel et al. 2005), only 15% of the stellar mass in the bulge was present by  $z \sim 1.5$ .

Infrared observations clearly show that the Galactic bulge hosts a prominent bar and that the bulge isophotes are “boxy” (e.g., Binney et al. 1991; Blitz & Spergel 1991; Dwek et al. 1995; see Figure 8). As noted by Kormendy & Kennicutt (2004), the only known mechanism for producing such a structure is secular evolution of the disk (bars are a disk phenomenon). However, the existence of a bar does not necessarily imply that the bulge contains young stars – it could have resulted from the perturbation of a pre-existing old disk. Even so, it is difficult to see how a bulge with a significant disk component would be consistent with the old and nearly coeval population favored by the chemical evolution models above.

Most recently, observations of galaxies at  $z \sim 2$ , i.e., at a lookback time comparable to the age of bulge stars, have opened new opportunities for understanding bulge formation processes. Integral field spectroscopy of several such galaxies with  $\sim 0.2$  arcsec ( $\sim 1$  kpc) resolution have revealed large, clumpy, rotating disks, with high velocity dispersion ( $\sim 70 - 100$  km s $^{-1}$ ), high star formation rate ( $\sim 100 M_{\odot}$  yr $^{-1}$ ), and very high gas fraction (Genzel et al. 2006, 2008; Bouché et al. 2007; Förster-Schreiber et al. 2008, in prep.). Such disks are likely to be prone to gravitational instability developing over a much shorter timescale compared to that of typical disks at  $z \sim 0$ , where instability was proposed to give rise to pseudo-bulges in a long-lasting secular evolution of disks (Kormendy & Kennicutt 2004). In addition to fast secular evolution of massive early disks, migration to the center and coalescence of their giant clumps has also been proposed for the fast formation of bulges in the early universe (Elmegreen et al. 2008). These unanticipated developments have significantly changed the traditional alternative between bulges originating via disk evolution, hence characterized by a broad distribution of stellar ages, and formation by massive bursts at early cosmic

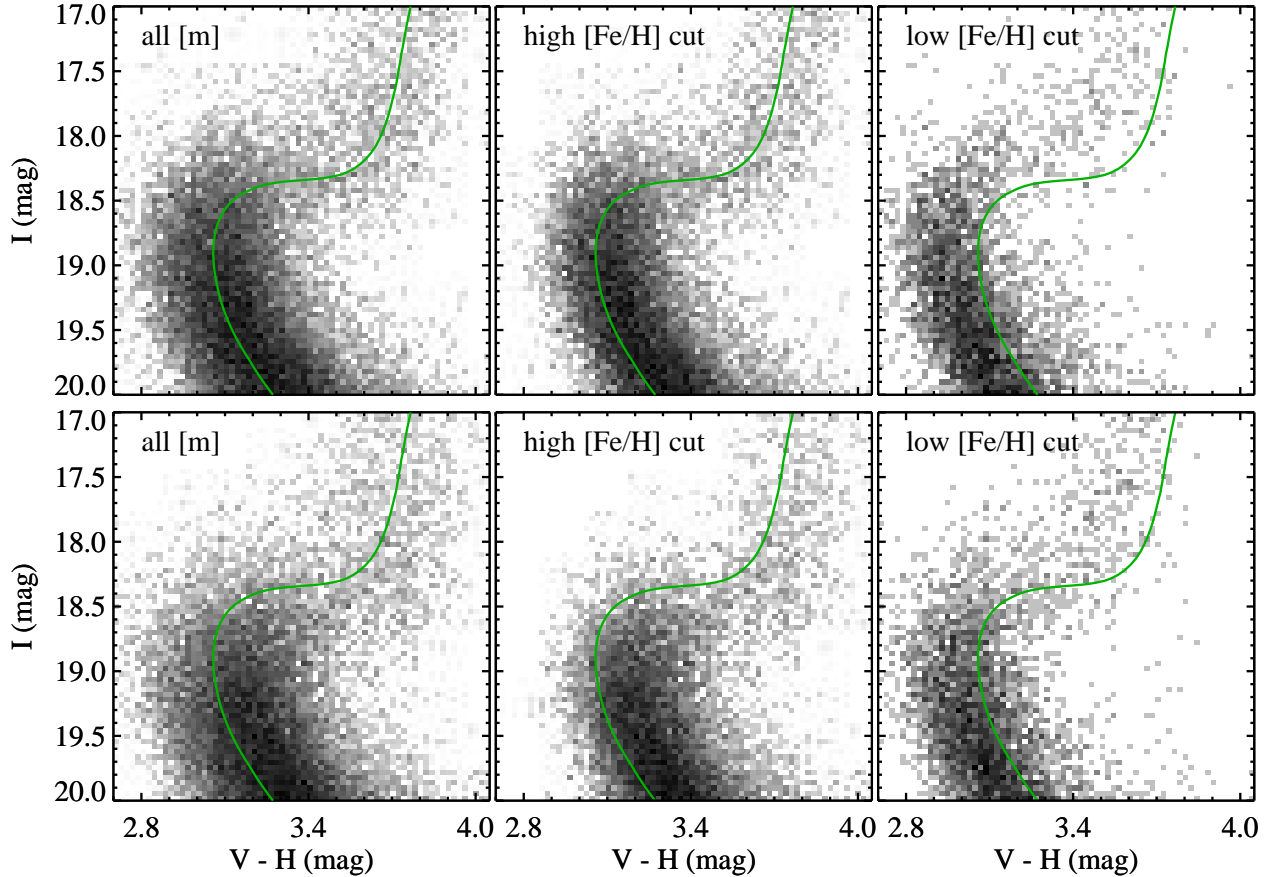


FIG. 7.— The same simulated populations shown in Figure 6 (top panels: extended star formation history; bottom panels: ancient coeval burst), but sorted into metallicity bins using cuts in the  $[m]$  vs.  $[t]$  plane: full catalog (left panels), metal-rich stars (middle panels), and metal-poor stars (right panels). Because the primary difference between the simulated populations is a shift of metal-rich stars from old to intermediate ages (see Figure 6), the distinction between the CMDs is most apparent when looking at the stars at high  $[Fe/H]$  (middle panels). Note that the spreads in extinction, distance, and age cause stars at distinct metallicities to overlap in CMD space.

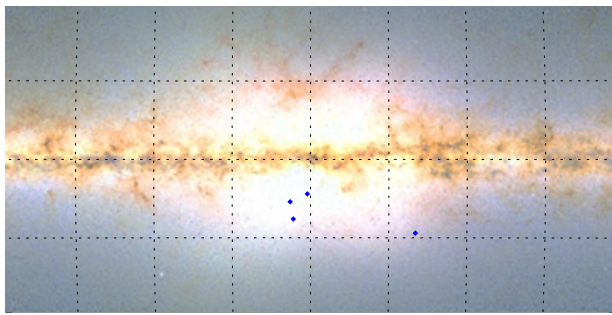


FIG. 8.— A 2MASS image (Skrutskie et al. 2006) with our bulge fields marked (blue diamonds) and a  $5^{\circ}$  grid shown for scale (dashed lines).

times, leading to uniformly old stellar ages. If  $z \sim 2$  disks are able to make bulges within a short timescale, then the Galactic bulge may well have formed in the same way, some 10 Gyr ago.

In addition to fast disk evolution at early times, a long lasting secular evolution may also follow at later times, funneling younger stars towards the bulge. If such a late time secular evolution plays a major role in the bulge, one might expect the age distribution to broaden as one moves from the bulge interior to its edges and corners. Although there is evidence of a metallicity gradient, such that metallicity decreases with increasing minor axis distance (Zoccali et al. 2008; Lecureur et al. 2008, in prep.), the existence of the metallicity gradient is disputed (Rich et al. 2007); furthermore, the existing data give no insight into any age gradient that might be present.

TABLE 2  
BULGE FIELDS

Name	$l$ (deg)	$b$ (deg)	$A_V$ (mag)	Reference
SWEEPS	+1.2559	-2.6507	2.0	Sahu et al. (2006)
Stanek's Window	+0.2508	-2.1531	2.6	Stanek (1998)
Baade's Window	+1.0624	-3.8059	1.6	Baade (1963)
OGLE29	-6.7532	-4.7195	1.5	Sumi (2004)

Studies of other spiral bulges in integrated light tend to show decreasing metallicity and increasing ages with increasing radius (e.g., Jablonka et al. 2007), but the statistical and systematic uncertainties in such work are large.

Because the bulge is largely obscured by dust, the Treasury program will target four well-studied low-extinction windows to sample diverse bulge fields: three near the minor axis and one in the corner of the boxy bulge (Table 2; Figure 8). The SWEEPS field (Sahu et al. 2006) has the deepest extant optical imaging in the bulge; it was observed with the ACS in the F606W and F814W filters, with followup to provide proper motions (Clarkson et al. 2008). Data from 2MASS (Two Micron All Sky Survey; Skrutskie et al. 2006) and OGLE (Optical Gravitational Lensing Experiment; Udalski et al. 2002) was used to judge the stellar density in the other fields relative to the SWEEPS field. The addition of a field in Stanek's Window (Stanek 1998) will allow a characterization of field-to-field variations in the bulge interior. The field in Baade's Window (Baade 1963) will provide a minor-axis measurement

closer to the edge of the boxy bulge. Finally, the OGLE29 field (Sumi 2004) is in one of the bulge corners. The OGLE29 field is also being imaged in a program using the High Acuity Wide-field  $K$ -band Imaging (HAWK-I) instrument on the Very Large Telescope (PI M. Zoccali). The HAWK-I images will each cover an area  $8\times$  larger than a WFC3 field, searching for any trace populations (at the level of a few percent) of young stars ( $<8$  Gyr), but without the sensitive age diagnostics possible with WFC3. The WFC3 program complements the HAWK-I program by obtaining the detailed star-formation history for the population in a bulge corner using the same photometric system employed in the interior. Proper motions of individual stars in these fields will enable both rejection of foreground disk stars and correlations of measured properties with bulge dynamics; as demonstrated by Clarkson et al. (2008), a  $1\sigma$  cut in proper motion space will reduce foreground disk contamination from  $\sim 10\%$  to less than 1%, yielding a nearly pure bulge population for study.

The Milky Way bulge is the only bulge where one can resolve the stars on the old main sequence, and this will be the situation for the foreseeable future. As such, the Galactic bulge is under intense scrutiny through a variety of experiments and theoretical modeling efforts exploring the stellar populations, dynamics, dark matter, and formation history. The WFC3 bulge Treasury program will produce catalogs that will be useful to such work, because its CMDs and proper motions will distill the stars into age, metallicity, and dynamical populations, and do so in 4 well-studied low-extinction windows spanning a range of bulge environments.

### 3.2. Jovian Planet Hosts in the Bulge

Over 300 extrasolar planets have been discovered to date, mostly via radial-velocity (RV) measurements, and more than 50 have been found via photometric transit surveys. One of the most surprising results of these searches has been the discovery of “hot Jupiters” – gas giants with orbital periods of just a few days. About 12 such planets were known before the SWEEPS (Sagittarius Window Eclipsing Extrasolar Planet Search) ACS survey. This transit survey continuously monitored a Galactic bulge field for 7 days, detecting 16 transiting hot Jupiter candidates (Sahu et al. 2006), including a new class of ultra-short-period planets (USPPs) orbiting with periods of 0.4–1.0 days around stars with masses less than  $\sim 0.9 M_\odot$ . Two of the brightest planet candidates were strengthened via RV followup measurements, but the remaining candidates are too faint and crowded for ground-based confirmation. The SWEEPS survey was performed in the F606W and F814W filters; while optimal for a transit search, these filters provide inadequate constraints on the metallicities of individual stars in the field (Figure 5), due to degeneracies in the ACS CMD.

The bulge Treasury program will accurately characterize the effective temperature and metallicity of 13 candidate planet hosts from SWEEPS, including 3 USPPs. Uncertainties of 0.2 dex in [Fe/H] and  $\lesssim 300$  K in  $T_{\text{eff}}$  will be obtained for 12 of these candidates, with errors twice as large for the 13<sup>th</sup>; the remaining 3 SWEEPS candidates fall outside the WFC3 field of view. The program will compare the metallicity distribution for hot Jupiter hosts with that of the general population, and do so in an environment with a wide metallicity range ( $-1.5 < [\text{Fe/H}] < +0.5$ ); it will also determine if the new class of USPPs forms preferentially around high-metallicity stars, as expected (Sahu et al. 2006; Ogilvie & Lin 2007). Metallicity measurements in the distinct bulge environment are an important complement to extrasolar planet studies in the solar neighborhood; the latter are mostly performed via RV measurements for stars at  $-0.5 < [\text{Fe/H}] < +0.5$ , and find that planet frequency is positively correlated with host metallicity (Fischer & Valenti 2005).

environment are an important complement to extrasolar planet studies in the solar neighborhood; the latter are mostly performed via RV measurements for stars at  $-0.5 < [\text{Fe/H}] < +0.5$ , and find that planet frequency is positively correlated with host metallicity (Fischer & Valenti 2005).

### 3.3. Metallicity Dependence of the Stellar Mass Function

In each of the bulge fields, the photometry will yield 0.2 dex errors in [Fe/H] for every star down to  $0.5 M_\odot$ , with coarser metallicity bins below this point (e.g., 0.4 dex errors in [Fe/H] at  $0.4 M_\odot$ ). Using *HST*, Zoccali et al. (2000) measured the bulge mass function down to  $0.15 M_\odot$  in a single bulge field; they found the mass function was close to Salpeter above  $\sim 0.5 M_\odot$ , but more shallow at lower masses. The bulge Treasury program will extend this earlier work by measuring the mass function as a function of metallicity and bulge environment, thus revealing how the characteristic mass of star formation varies with chemistry. Investigating the metallicity dependence of the stellar mass function in a field population, such as the bulge, may give a better indication of the “initial” mass function than studies that focus on globular clusters. Globular clusters generally offer clean samples at a single age and metallicity, but the low-mass end of the mass function they provide has been significantly distorted by dynamical processes.

### 3.4. Proper Motions in the Bulge

Proper motions of individual stars in these fields will enable both rejection of foreground disk stars and correlations of measured properties with bulge dynamics; as demonstrated by Clarkson et al. (2008), a  $1\sigma$  cut in proper motion space will reduce foreground disk contamination from  $\sim 10\%$  to less than 1%, yielding a nearly pure bulge population for study. One of the four bulge fields (SWEEPS) already has proper motions with  $0.3 \text{ mas yr}^{-1}$  accuracy (Clarkson et al. 2008) from deep multi-epoch ACS images spanning a two-year baseline. The WFC3 images will be deeper than the second epoch ACS images of the SWEEPS field, and will increase the proper motion baseline from 2 years to at least 5 years, thus significantly reducing the uncertainties in individual proper motion measurements. For brighter stars ( $I \lesssim 24$  mag), the errors in proper motions will be reduced by a factor of  $\sim 2.5$ , but this increased accuracy will do little to assist the bulge-disk separation for such stars, because the measurement uncertainties are already significantly smaller than the motions themselves. For fainter stars, the uncertainties in proper motions are significant compared to their motions, driven by large astrometric uncertainties in the second epoch. With the deep WFC3 images, the reduction in errors for these stars will be larger than 2.5, varying with brightness, which will improve the bulge-disk separations. This will be particularly helpful in investigating the apparent discrepancy between the theoretical isochrones and the observed CMD at these fainter magnitudes.

For the other three bulge fields, the Treasury program will spend three orbits to obtain a second epoch of F814W imaging and thus proper motions to the same accuracy. Extant shallow ACS mosaics (using the F435W, F625W, and F658N filters) can be used with the WFC3 images to obtain preliminary proper motions in 2 of these fields (in Baade’s Window and Stanek’s Window), but these will be hampered by differences in depth, geometric distortion, plate scale, and bandpass. The primary purpose of proper motions will be to screen the foreground disk stars, but the accuracy will be sufficient

to study the bulge dynamics, complementing existing radial velocity measurements. The current kinematic picture of the Galactic bulge (see Minniti & Zoccali 2007 and references therein) shows it to be intermediate between a rotationally-supported system (such as the disk) and a pressure-supported system (such as the halo), but the Treasury program will extend these measurements along the minor axis and to a corner of the boxy bulge.

#### 4. SUMMARY

With its broad wavelength coverage, high spatial resolution, rich filter set, and wide field of view, WFC3 brings powerful new stellar population tools to *HST*. Taking advantage of these capabilities, the new five-band photometric system described here will enable the construction of reddening-free indices of metallicity and temperature. With these indices, observers can fit the star formation history in a population by modeling the distribution of stars in the  $T_{\text{eff}}$ -[Fe/H] plane, avoiding the reddening uncertainties arising in traditional CMD fitting. Although this system was designed with the specific goal of understanding the formation of the Galactic bulge, it should be useful to a wide range of stellar populations.

#### REFERENCES

Baade, W. 1963, Evolution of Stars and Galaxies (Cambridge: Harvard University Press), 277

Ballero, S.K., Matteucci, F., Origlia, L., & Rich, R.M. 2007, *A&A*, 467, 123

Binney, J., Gerhard, O.E., Stark, A.A., Bally, J., & Uchida, K.I. 1991, *MNRAS*, 252, 210

Blitz, L., & Spergel, D.N. 1991, *ApJ*, 379, 631

Bouché, N., et al. 2007, *ApJ*, 671, 303

Brown, T.M., et al. 2005, *AJ*, 130, 1693

Brown, T.M., Smith, E., Ferguson, H.C., Rich, R.M., Guhathakurta, P., Renzini, A., Sweigart, A.V., & Kimble, R.A. 2006, *ApJ*, 652, 323

Castelli, F., & Kurucz, R.L. 2003, in IAU Symposium 210, Modeling of Stellar Atmospheres, eds. N. Piskunov, W.W. Weiss, & D.F. Gray, poster A20, astro-ph/0405087

Clarkson, W., et al. 2008, *ApJ*, accepted

Cole, A.A., et al. 2007, *ApJ*, 659, L17

De Lucia, G., & Blaizot, J. 2007, *MNRAS*, 375, 2

Dwek, E., Arendt, R.G., Hauser, M.G., Kelsall, T., Lisse, C.M., Moseley, S.H., Silverberg, R.F., Sodroski, T.J., & Weiland, J.L. 1995, *ApJ*, 445, 716

Dolphin, A.E. 2002, *MNRAS*, 332, 91

Elmegreen, B.G., Bournaud, F., & Elmegreen, D.M. 2008, *ApJ*, in press, arXiv/0808.0716

Ferreras, I., Wyse, R.F.G., & Silk, J. 2003, *MNRAS*, 345, 138

Fischer, D.A., & Valenti, J. 2005, *ApJ*, 622, 1102

Fitzpatrick, E.L. 1999, *PASP*, 111, 63

Gallart, C., Freedman, W.L., Aparicio, A., Bertelli, G., & Chiosi, C. 1999, *AJ*, 118, 2245

Genzel, R., et al. 2006, *Nature*, 442, 786

Genzel, R., et al. 2008, *ApJ*, in press, arXiv/0807.1184

Harris, J., & Zaritsky, D. 2001, *ApJS*, 136, 25

Harris, J., & Zaritsky, D. 2004, *AJ*, 127, 1531

Holtzman, J.A., et al. 1999, *AJ*, 118, 2262

Iben, I., & Renzini, A. 1984, *PhR*, 105, 329

Johnson, H.L., & Morgan, W.W. 1953, *ApJ*, 117, 313

Jablonka, P., Gorgas, J., & Goudfrooij, P. 2007, *A&A*, 474, 763

Kormendy, J., & Kennicutt, R.C. 2004, *ARA&A*, 42, 603

Mihalas, D., & Binney, J. 1981, Galactic Astronomy (New York: W.H. Freeman and Company), 186

Minniti, D., & Zoccali, M. 2007, Galactic Bulges (San Francisco: ASP), astro-ph/0710.3104

Ogilvie, G.I., & Lin, D.N.C. 2007, *ApJ*, 661, 1180

Rattenbury, N.J., Mao, S., Debattista, V.P., Sumi, T., Gerhard, O., & De Lorenzi, F. 2007, *MNRAS*, 378, 1165

Rich, R.M., Origlia, L., & Valenti, E. 2007, *ApJ*, 665, L119

Sahu, K., et al. 2006, *Nature*, 443, 534

Sandage, A. 1982, *ApJ*, 252, 553

Skrutskie, M.F., et al. 2006, *AJ*, 131, 1163

Springel, V., et al. 2005, *Nature*, 435, 629

Stanek, K.Z. 1998, *ApJL*, submitted, astro-ph/9802307

Stetson, P. 1987, *PASP*, 99, 191

Strömgren, B. 1966, *ARA&A*, 4, 433

Sumi, T. 2004, *MNRAS*, 349, 193

Udalski, A., Szymanski, M., Kubiak, M., Pietrzynski, G., Soszynski, I., Wozniak, P., Zebrun, K., Szewczyk, O., & Wyrzykowski, L. 2002, *Acta Astron.*, 52, 217

VandenBerg, D.A., Bolte, M., & Stetson, P.B. 1990, *AJ*, 100, 445

VandenBerg, D.A., Bergbusch, P.A., & Dowler, P.D. 2006, *ApJS*, 162, 375

Zoccali, M., Cassisi, S., Frogel, J.A., Gould, A., Ortolani, S., Renzini, A., Rich, R.M., & Stephens, A.W. 2000, *ApJ*, 530, 418

Zoccali, M., et al. 2008, *A&A*, 486, 177

Zoccali, M., Renzini, A., Ortolani, S., Gregg, L., Saviane, I., Cassisi, S., Rejkuba, M., Barbuy, B., Rich, R.M., & Bica, E. 2003, *A&A*, 399, 931